Prediction of reservoir characterization using seismic post-stack inversion and neural network analysisin Wadi Rayan Field, Western Desert, Egypt

M. Fathy*

*Geology Department, Faculty of Science, Al Azhar University, Cairo, Egypt.
E-mail: green_geophysics@yahoo.com

Abstract: The Abu Roash G member is a Cenomanian in age and the only producing horizon in this area; it's composed of shale and sandstones intercalations with minor carbonate interbeds. The main producing interval in this member is ARG-5 which consists of sandstone, silt and shale. The thickness varies along the whole survey area. There are two intervals of producing sandstone which not only vary from well to another, but also not deposited in some wells. For these causes, it is important to incorporate all available geological and geophysical data to come upward with a model for ARG reservoir. The first Model-based inversion makes use of an initial geologic model, based on the impedance data, structural information and wavelet extracted. The second Neural network analysis is one of these algorithms. It uses the data from multiple wells and seismic information to prepare a neural net to predict properties away from the well control and to delineate the ARG reservoir for more exploration and development opportunities.
[M. Fathy. **Prediction of reservoir characterization using seismic post-stack inversion and neural network analysis in Wadi Rayan Field, Western Desert, Egypt.** *Nat Sci* 2016;14(1):78-93]. ISSN 1545-0740 (print); ISSN 2375-7167 (online). http://www.sciencepub.net/nature. 10. doi:10.7537/marsnsj14011610.

Keywords: Wadi Rayan, ARG-5, Inversion, Neural network.

1. Introduction

The Wadi Rayan field is placed about 71.5 mils (115 Km.) Southwest Cairo, between: Latitudes 29° 00' 00" and 29° 30' 00" N and Longitudes 30° 00' 00" and 31° 00' 00" E The elevation of this region ranges between -36 to 210 foot. (-11 to +64 meters) mean sea level Figure 1.It was discovered in Sep., 1996 through drilling well WR-1x which has been drilled to a total depth of 7740 foot in Basement. A thick sandstone body of (100 ft). Net sandstone of Abu Roash G member has been tested oil with rate of 996 BOPD on 64/64" chock size. The Crude is characterized by a moderately low API gravity (26 API) and low pour point (100F). The study area is a platform lying between Abu Gharadig and Benisuef basins.

1.1 Stratigraphy

The sedimentary sequence of the Wadi El-Rayan Field ranges in age from the Lower Cretaceous to Middle Eocene Figure 2. The sedimentary section in the Wadi El-Rayan province is characterized by the absence of the Paleozoic and Jurassic rocks as a resolution of non-deposition on the Wadi El-Rayan platform. A thin Lower Cretaceous section was deposited at once over the Precambrian basement rocks (Said1990, Hantar, 1990, EGPC, 1992 and Abdel Aziz *et al.,* 1998).

1.2 Structure

The Western Desert of Egypt consists of a series of small rift basins. More or less of them dated back to the Permian, but the majority can be believed to have originated during the Late Jurassic-Early Cretaceous, contemporaneously with the foundation of the Mediterranean basins. Despite a relatively complex story, the geological framework of Egypt is highly suited for petroleum and gas exploration. It contains eight major tectono-stratigraphic events:

(Paleozoic craton, Jurassic rifting, Cretaceous passive margin, Cretaceous Syrian arc deformation and foreland transgressions, Oligo-Miocene Gulf of Suez rifting, Miocene Red Sea breakup, The Messinian salinity crisis and Plio-Pleistocene delta progradation. Each of these issues has created multiple reservoir and seal combinations. Source rocks occur from the Paleozoic through to the Pliocene and petroleum is produced from Precambrian through Pleistocene age reservoirs (Dolson, 2000). Seismic and borehole data indicate that the Jurassic and Cretaceous (mainly Lower Cretaceous) rocks were deposited in rift basins in the Northern Western Desert. These basins had the form of half-grabens, each bounded by a major fault on its down dip side. Away from this fault, the dip angle of the rocks within the basin decreases and at the extreme up the dip edge of the basin they have a very gentle dip and are usually referred to as platforms by several investigators, e.g. Sitra and Wadi El Rayan platforms (Moustafa, 1988 and 2008).The area under consideration is located within the northern Egypt folds belt that is part of the Syrian Arc System.After the deposition of the Cenomanian-Turonian; and Lower Senonian rocks; folding and reverse faulting affected the Abu Roash Formation and older rocks as well as the lower part of the Khoman Formation. The structures of study area include both folds and faults.

Folds in Wadi EL-Rayan platform are symmetric and have gentle dipping flanks and have a NE-SW orientation (Krenkel, 1925). They are oriented ENE-WSW, NE-SW and NW-SE. The oriented faults are predominantly normal and were active at least two times. These faults were active in the Early and Late Cretaceous time (Abdelazi*et al.,* 1998). From seismic data interpretation construct a map on top A/R (G) member affected by both normal and reverse faults. ENE-WSW trend caused by rifting in late Jurassic which continued to early Cretaceous in the northern part of the Western Desert and reactivated in late Cretaceous in study area Figure 3 and showing that in seismic section Figure 4.

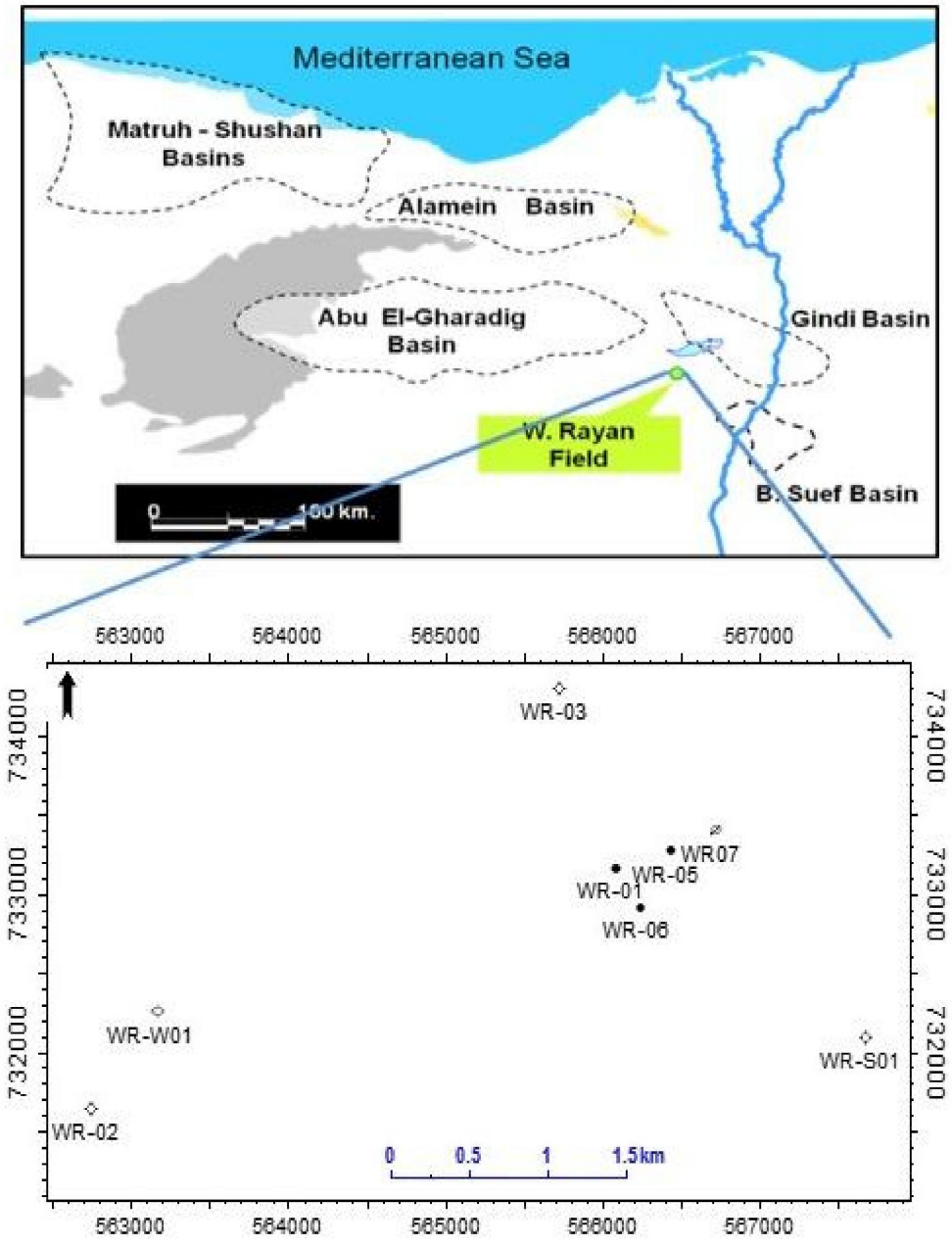

Figure 1. Index map showing the locations of the Wadi Rayan Field which lying between Abu Gharadig Basin and Gindi Basin, Western Desert, Egypt.

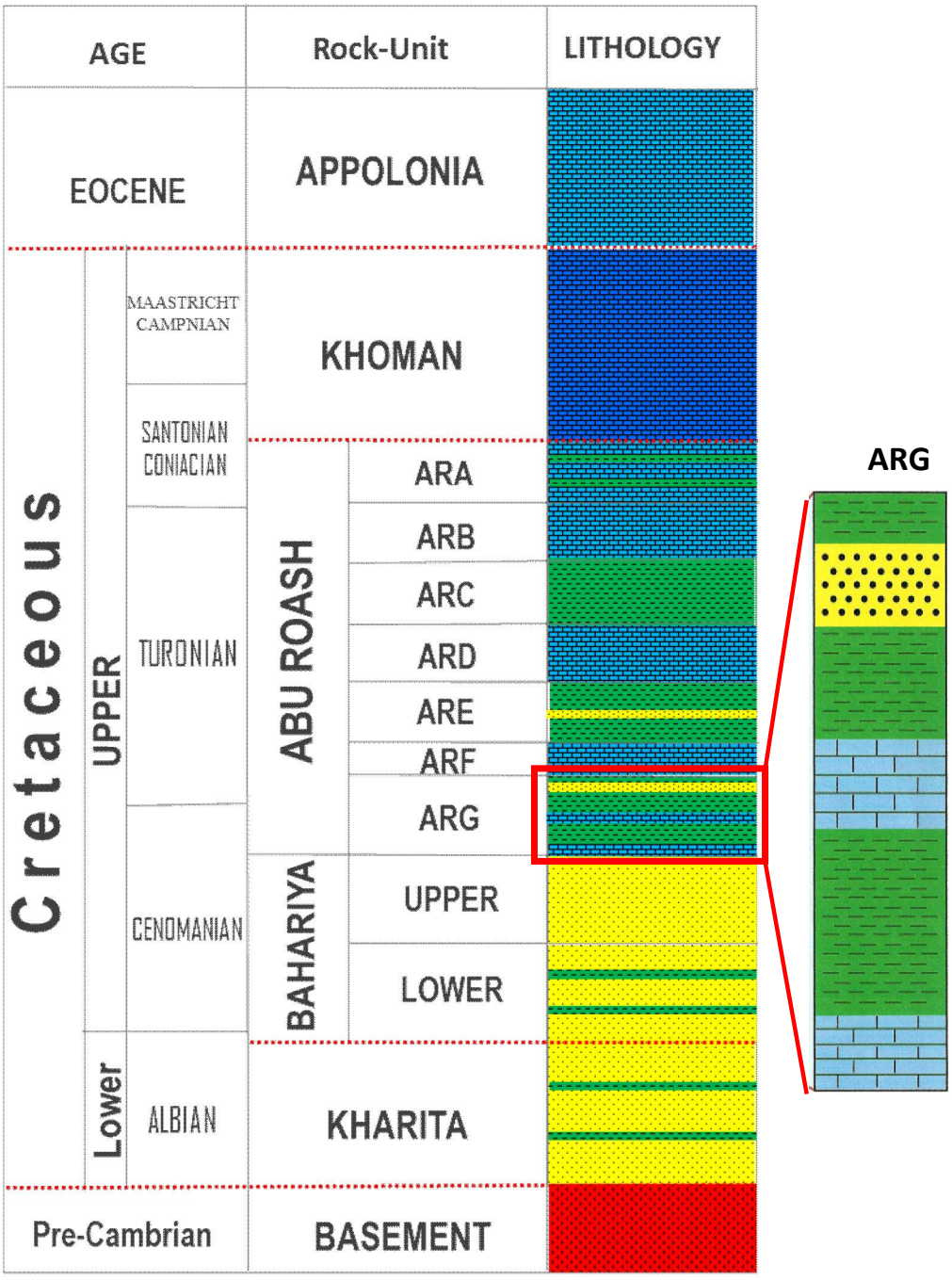

Figure (2): Wadi El-Rayan Stratigraphic column from available well log data.

Methods

Post-stack inversion is a good tool to estimate elastic properties. Nevertheless, the model parameters and the wavelets' estimation accuracy significantly affect the final inversion results. The neural network estimation of the reservoir properties proved the accuracy and consistency with the well logs, which might compensate for the inversion parameters' uncertainty show that in (Figure 5 and Figure 6).

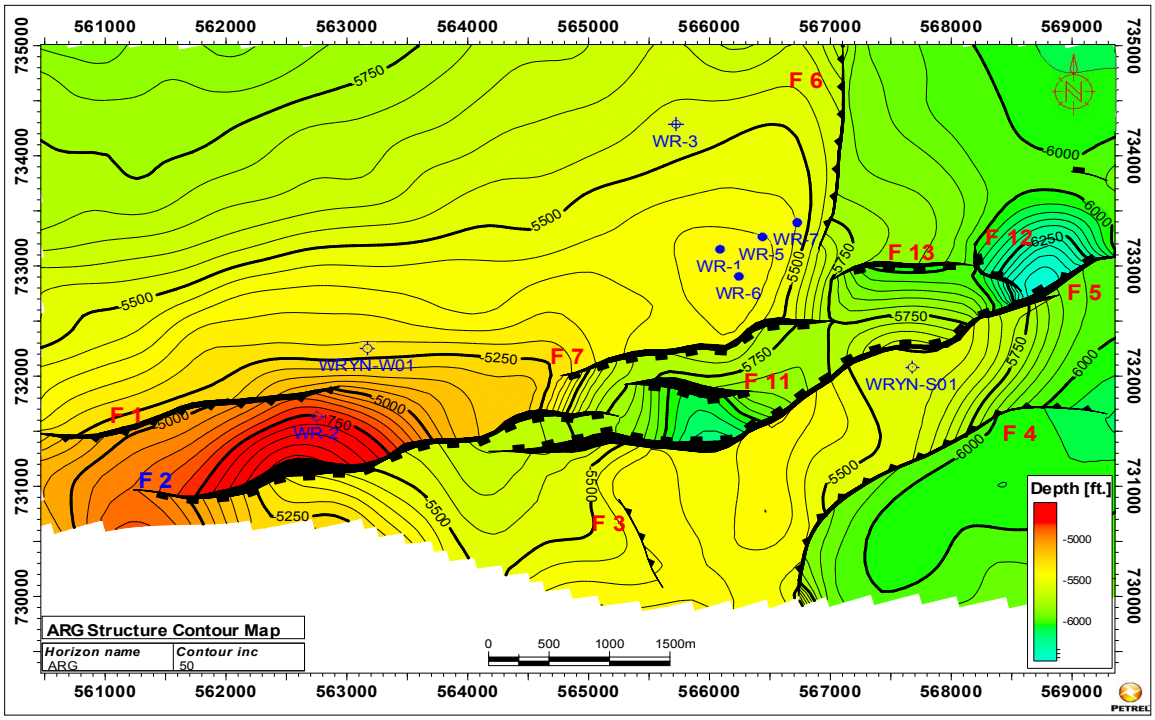

Figure (3): Depth Structure Map on the Top ARG in the Wadi Rayan Field showing fault trends and the surface topography.

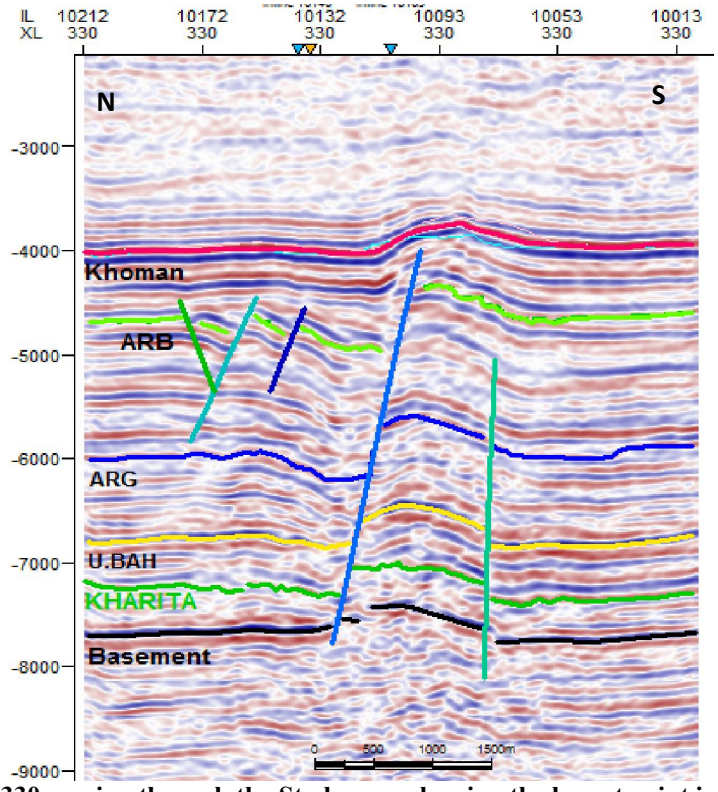

Figure (4): X-line 330 passing through the Study area showing the lowest point in the ARG.

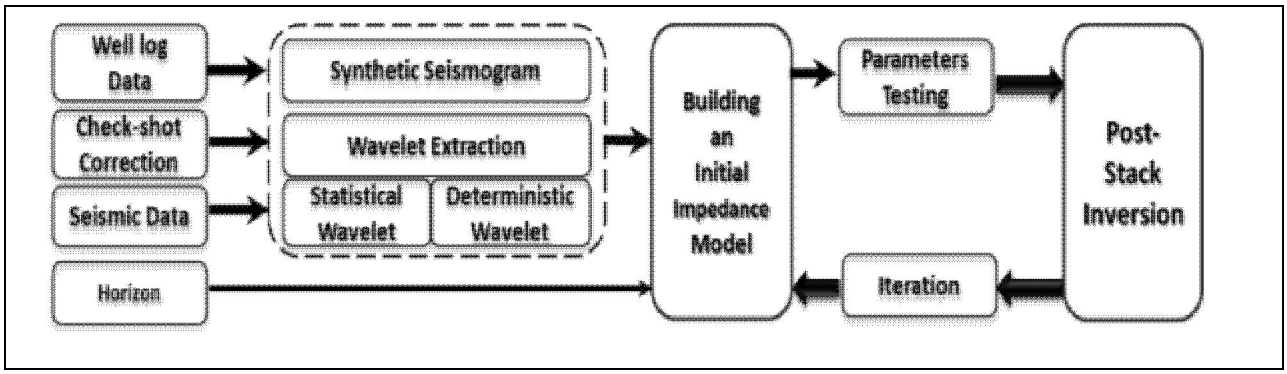

Figure (5): Flow chart showing the steps of Post-stack inversion

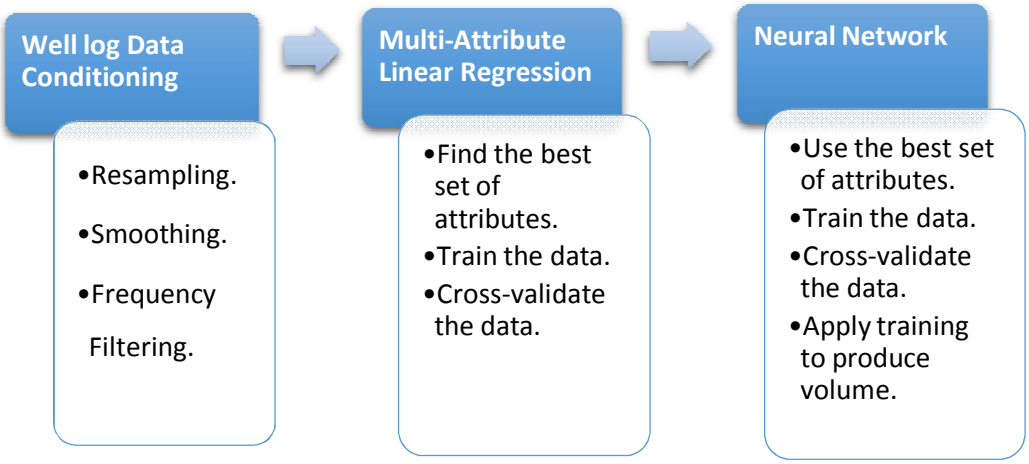

Figure (6): Neural Network Workflow.

2 Seismic Inversion technique in Wadi Rayan Field

Seismic inversion is recovering earth properties from seismic data (Russell and Hampson, 2006) in order to elicit additional information (Veekan and Silva, 2004).Several cases of inversion have been set over the years each with their own strong points and restrictions. Input data required for an inversion includes; time-migrated pre/post-stack data, a wavelet, an initial earth model and picked horizons in TWT (Veekan and Silva, 2004). Inversion results show higher resolution and documentation more accurate interpretations (John Pendrel, 2001). This technique popularized by BP some 10 years ago (Lancaster and Whitcombe, 2000) is one where an operator is designed to map the seismic spectrum onto an earth spectrum typically derived from well data. No wavelet is required, and colored inversion cannot be used simultaneously on multiple partial stacks. It is of the essence to ensure the seismic is zero phase (Kemper 2010).

2.1 Statistical Wavelet Extraction

2.1.1 The statistical wavelet extraction

The process uses the seismic traces alone (auto-correlation). The phase spectrum is not computed by this method and must be provided as a separate parameter by the user. The wavelet estimation is performed in the time window where the match between seismic and synthetic reflectivity seems the more reliable (Figure 7 and Figure 8).

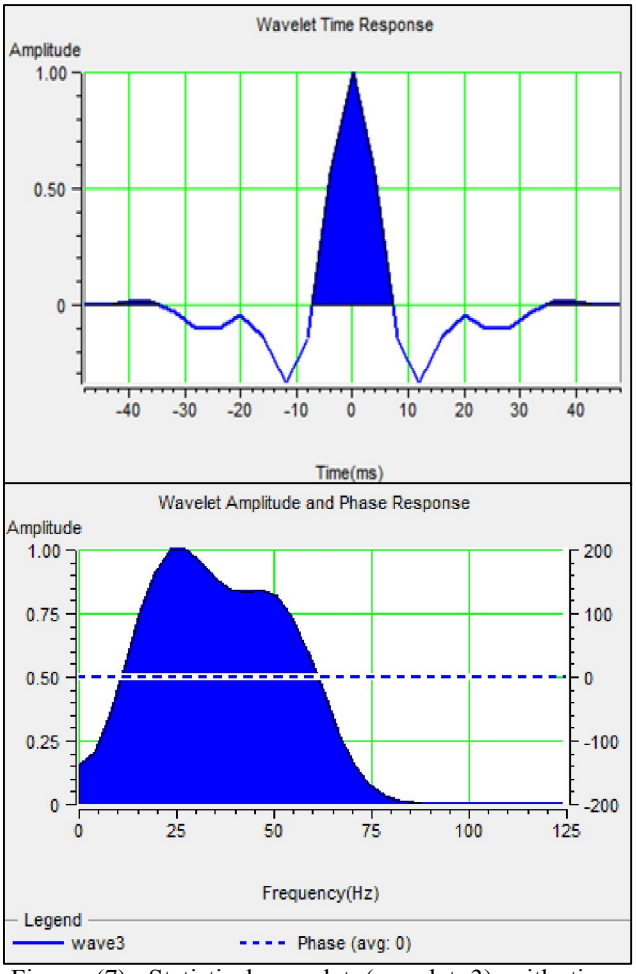

Figure (7): Statistical wavelet (wavelet 3) with time response on top and respective amplitude spectrum on the bottom. The phase is constant 0 degree.

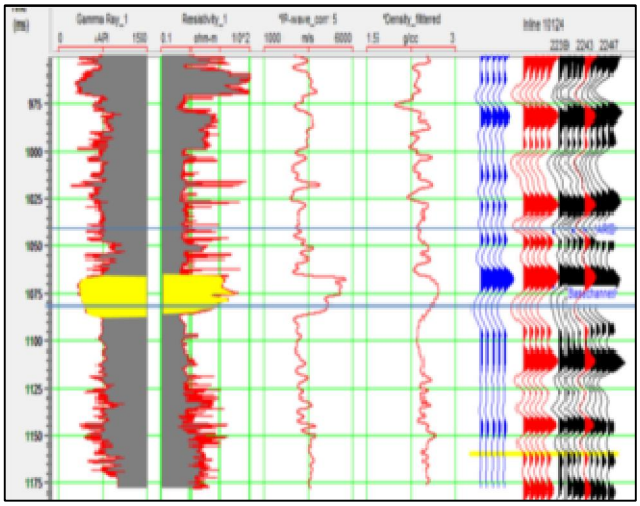

Figure (8): the well ties in WR-6 well. The logs (from left. to right) are, GR, Resistivity, P-wave and Density. The blue seismic trace is the calculated synthetic and the red is the real seismic data respectively, using the previous statistical wavelet.

2.1.2 Deterministic Wavelet Extraction

The deterministic wavelets were estimated by working out a matching operator between the seismic data and the reflectivity series in the frequency field.Several operators were extracted on different time windows and seismic traces. The validity of the extracted wavelets was checked by convolving them to the reflectivity series, followed by cross-correlation between the new synthetic data with the seismic traces surrounding the relevant well (Figure 9 and Figure 10).

2.2 Initial Model Building

Seismic data losses both the high and low frequencies and hence, the resulted impedance will not contain this missed data so, the impedance can't be fixed by using stacked seismic data alone. The input required for creating the initial model will be well-log data too, the stacked seismic data. The initial estimate of the reservoir properties is provided by the low frequency trend of the well logs: VP, and density. The interpolation between well logs will use the inverse distance Power algorithm with exponent value 3. The initial model was specified by six wells (WR-1, WR-2, WR-6, WR-7, WR-S01, WR-W01) and a set of horizons obtained from structural interpretation, including six horizons; Khoman, ARA, ARC, ARG, UBAH, Basement.WR-5 was a blind well, which removed from making the initial model in order to corroborate the initial model that well used as an input to inversion process. Consider (Figure11).

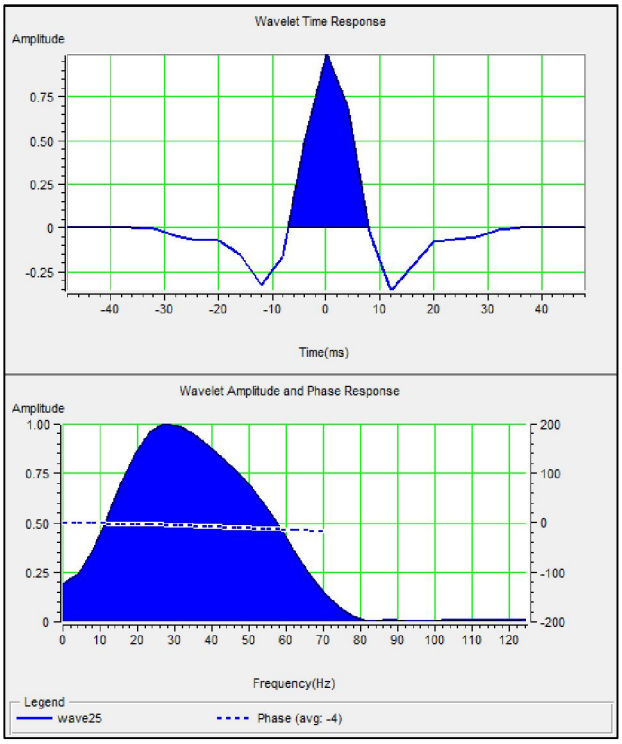

Figure (9): Deterministic wavelet (wavelet 25) with time response on top and respective amplitude spectrum on the bottom.

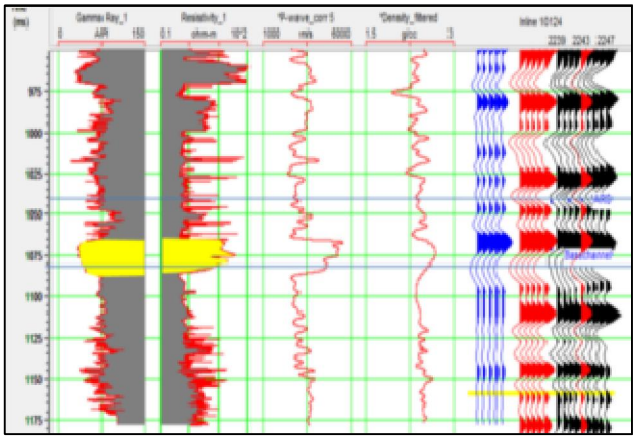

Figure (10): An example of the well ties in WR-6 well. The logs (from left. to right) are, GR, Resistivity, P-wave and Density. The blue seismic trace is the calculated synthetic and the red is the real seismic data respectively, using the previous deterministic wavelet.

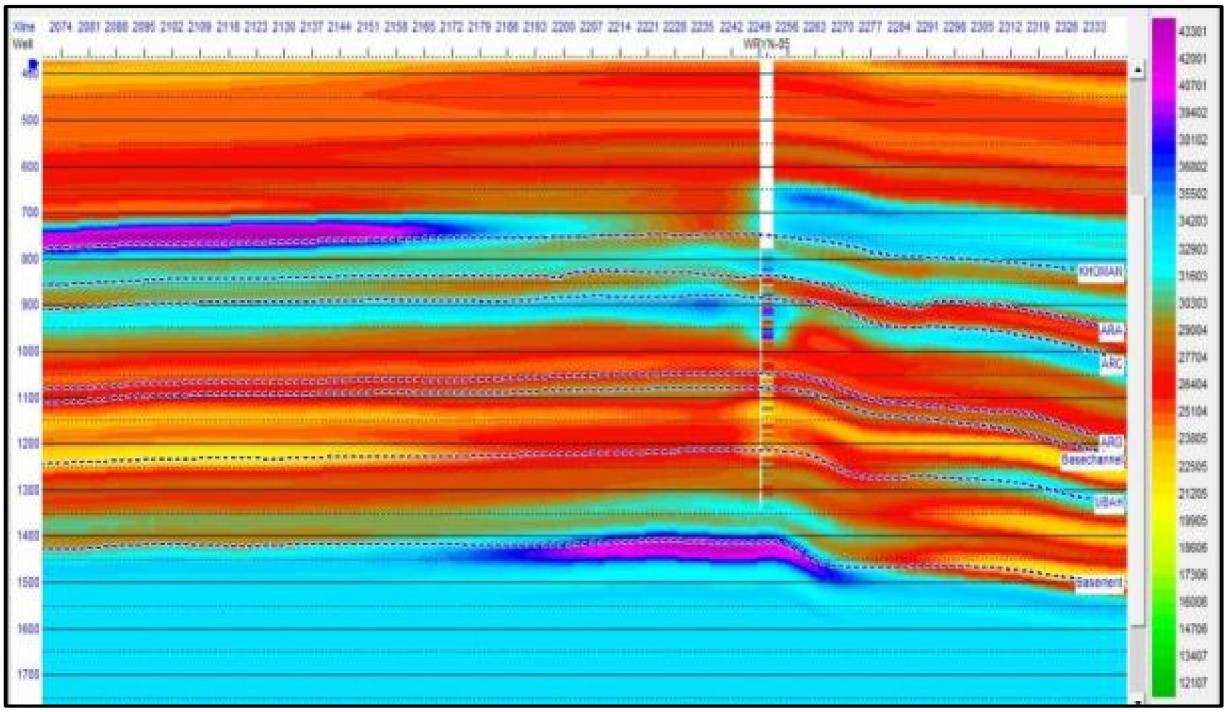

Figure (11): Showing a blind well (WR-5) which was removed during constructing the initial model.

2.3 Post-Stack Inversion

While the pre-stack inversion estimates P-impedance (Zp), S-impedance (Zs), VP/Vs and density (ρ) volumes, the post-stack Inversion estimates only P-Impedance. In this study, Model-Based and Colored inversion will be enforced.

2.3.1 Model-Based Inversion

Model-Based inversion allows us to use well data which contains both low and high frequency that missed in seismic Data. Another advantage in model-based method that it permits us to incorporate into the seismic interpretation a model, based on the known or suspected geology. This can result in better resolvability and a better link between the seismic data and the actual lithology. The work flow goes from an initial low frequency model of P-wave velocity and density. As the program iterates, it improves the fit between the recorded seismic traces and model-based synthetic traces by locally modifying the P-impedance model together with local deviations of the relationship between P-impedance and density. Figure 12 shows the post-stack inversion workflow. After making the initial model, the deterministic wavelet was used to invert the seismic cube. Before inverting seismic, inversion analysis has been prepared to see the error values and correlation coefficients, see table 1 and (Figure 13).

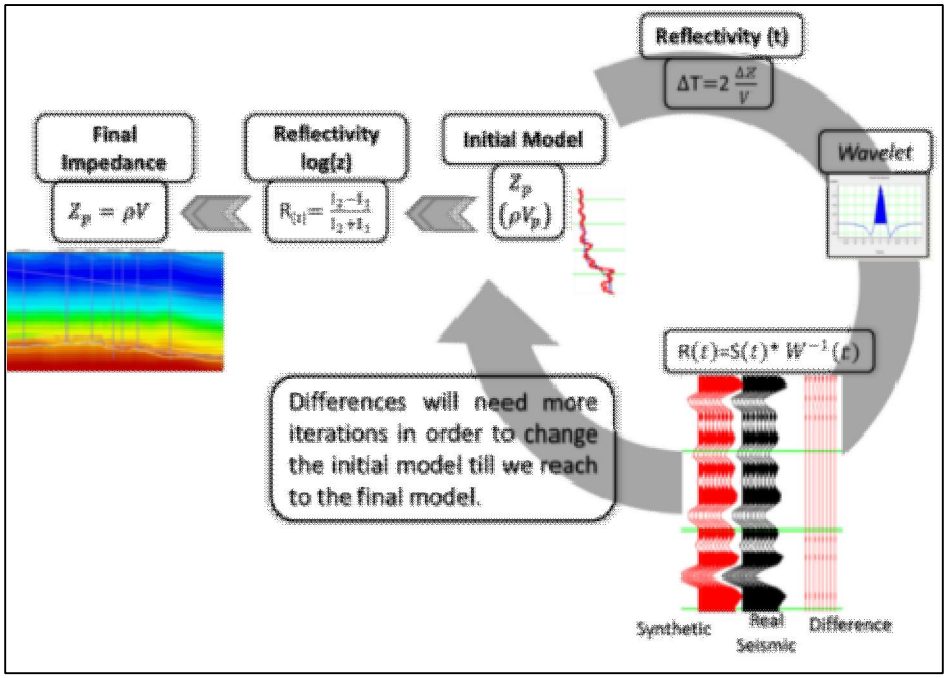

Figure (12): A schematic showing Workflow for post-stack inversion.

Table (1): Error values between the inverted and the original well logs and the correlation coefficients between the original and synthetic seismic data. theZp error % calculated by using the following equation: Zp error %= (Zp error value/ seismic max Zp)*100.

Well	*Zp Error*		*Correlation Coefficient*	*Synthetic error*
	Value	%		
WR-1	4597.5	6.87	0.9998	0.0186
WR-2	3435.07	5.14	0.9998	0.021
WR-5	5121	7.66	0.9999	0.01125
WR-6	4856.73	7.26	0.999852	0.0183292
WR-7	5002	7.48	0.999928	0.01515
WR-S01	6195	9.26	0.99816	0.06471
WR-W01	4985	7.45	0.999798	0.021687

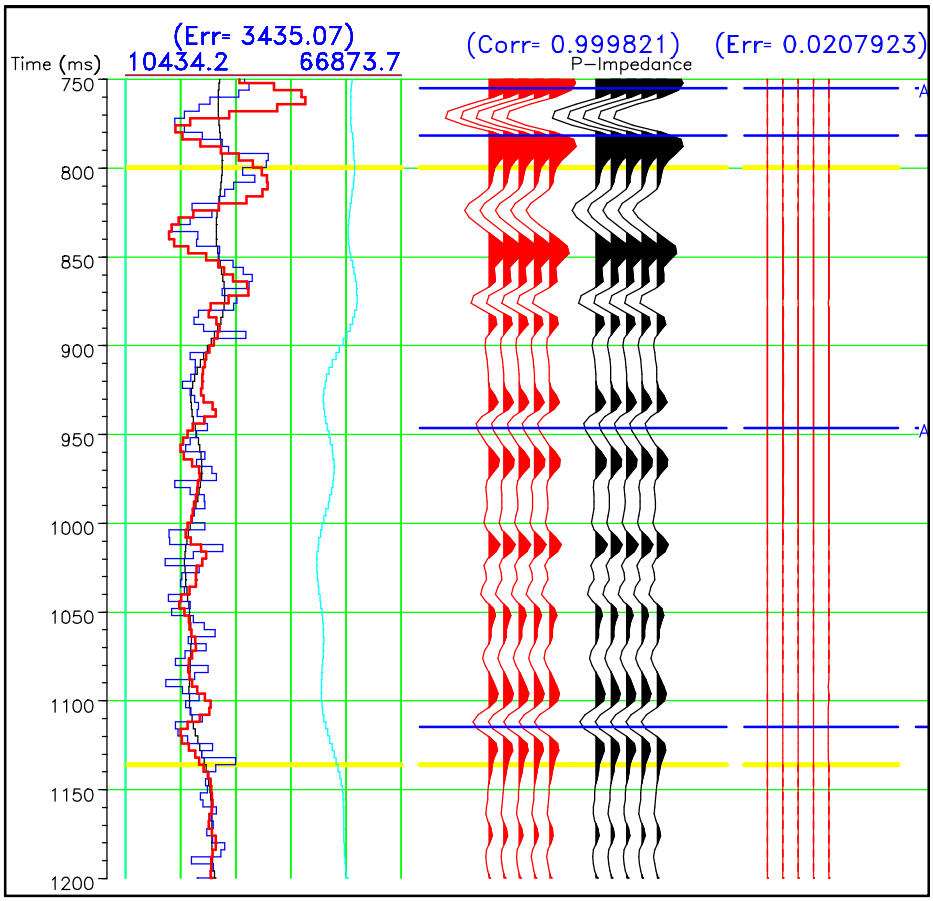

Figure (13): Post-stack inversion analysis for well WR-2 using deterministic wavelet. From Left to Right the columns represent the inverted Zp, (red) compared with original logs (blue). The Synthetic trace created by the inversion is shown in red and the original seismic trace is shown in black. The difference between the two is shown by the log on the far right. The inversion analysis was done for the reservoir interval in ARG. the inversion analysis window marked by yellow.

2.3.2 Colored Inversion

It applies an operator in the frequency domain to a seismic trace to transform it into impedance. It is a fast method and therefore good for a first look inversion. It also does not need a good initial model. First, we will derive the Operator spectrum by plotting AI for wells Vs Frequency; we can fit a straight line which represents the "desired" output impedance spectrum. Then, by using a set of seismic traces from around the wells, the average seismic spectrum is calculated. From the two preceding spectra, the operator spectrum is calculated. This has the effect of shaping the seismic spectrum to the impedance spectrum within the seismic band Figure 14. After that, putting together the derived amplitude spectrum with the -90 degree phase shift produces the Colored Inversion Operator. Finally, convolve this operator with seismic to produce the colored inverted cube, Figure 15.

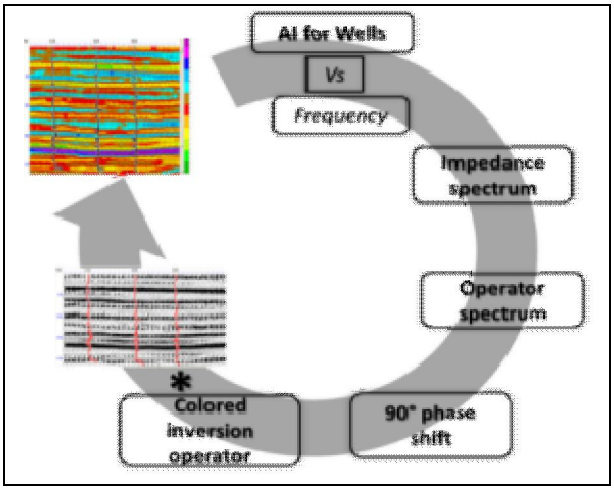

Figure (14): Colored inversion workflow (modified after Whitcombe, 2000)

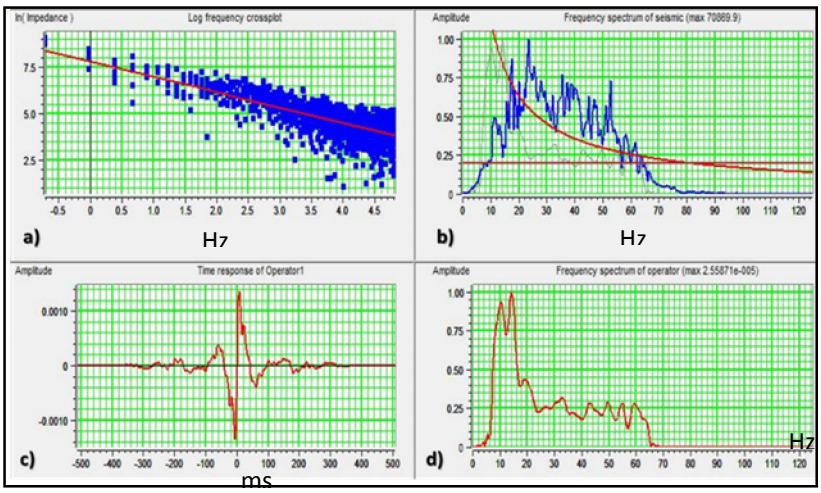

Figure (15): Showing the deriving of operator spectrum. a) The Impedance spectrum versus frequency. The red line representing the desired" output impedance spectrum. b) The average seismic spectrum is calculated from traces around the wells (blue), the desired" output impedance spectrum (red). c) Calculated operator which will convolve to seismic. d) Calculated operator spectrum.

2.4 Inversion Results

In this study, two methods of post-stack inversion were used which were Model-Based and colored inversion. The final results from the Model-Based inversion consisted of one cube of P-impedance (Zp) Figure 16.

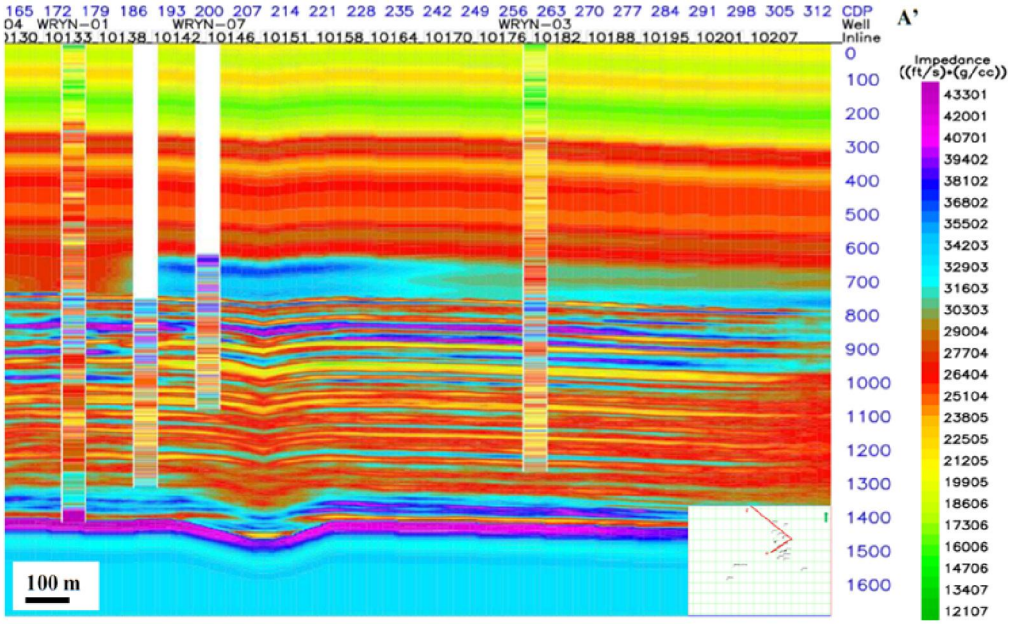

Figure (16): Arbitary line for post-stack inversion results showing p-impedance (Zp) with p-impedance log curves at each well.

2.4.1 Model-Based Inversion Results

In this segment I will represent the inversion results for Model-Based Inversion by running horizon slices attributes.This Figure (17 and 18) shows the presences of high P-impedance areas in the central part (B) and (C) which have hydrocarbon saturation and contain producer wells like WR-1, WR-5 and have a good structural trap but not all producer wells inside this trap. This impedance looks like two branches oriented NNE-SSW and NNW-SSE. In addition, there are two areas (A) and (D) to the west and to the east of producer wells, respectively, which give a high impedance that, could contain hydrocarbon but stratigraphically trapped.

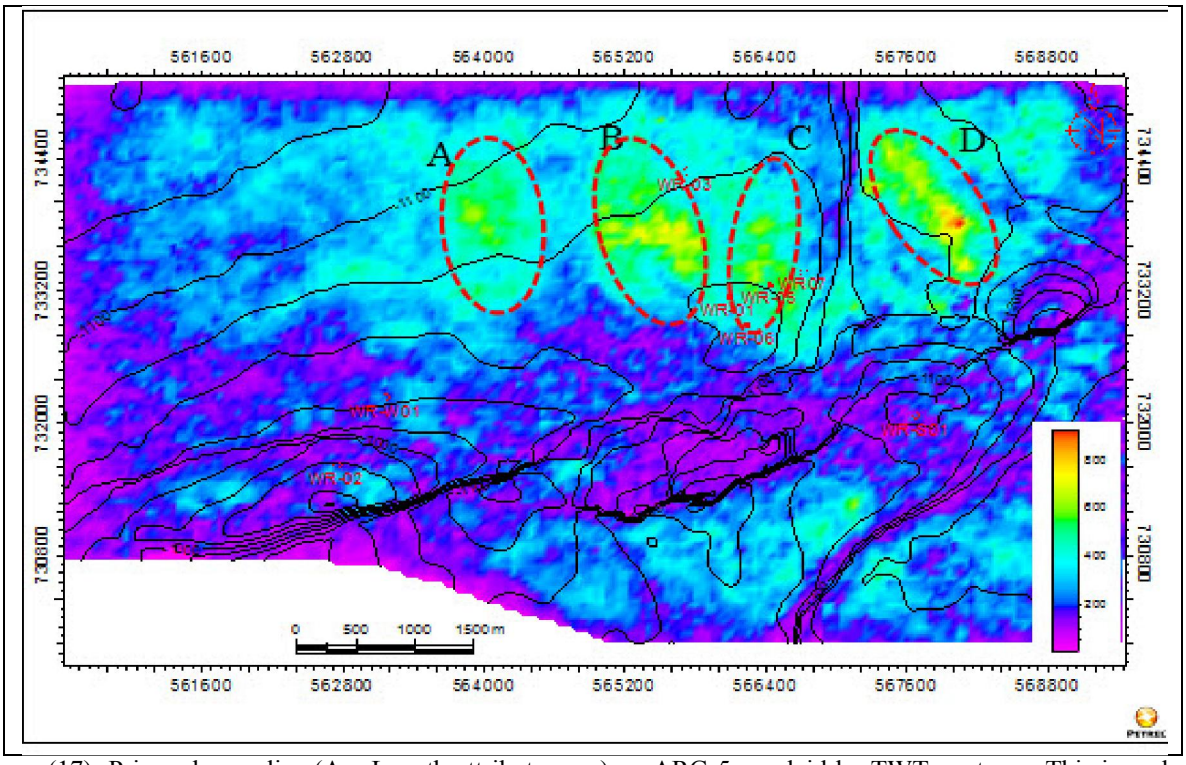

Figure (17): P-impedance slice (Arc Length attribute map) on ARG-5 overlaid by TWT contours. This impedance looks like two branches oriented NNE-SSW and NNW-SSE. In addition, there are two areas (A) and (D) to the west and to the east of producer wells respectively, which give high impedance that, could contain hydrocarbon but stratigraphically trapped.

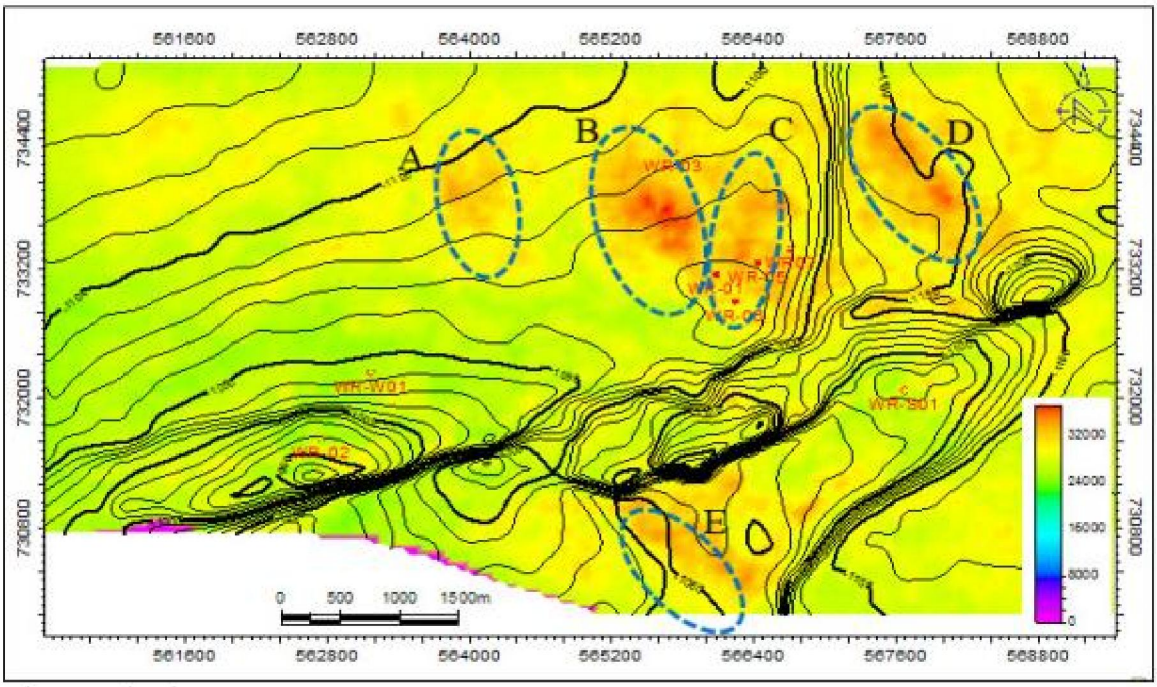

Figure (18): P-impedance slice (Maximum Amplitude) on ARG-5 overlaid by TWT contours. The maximum amplitude occurs in areas (B) and (C) which have hydrocarbon saturation and contain producer wells like WR-1, WR-5 while WR-2, WR-S01 are dry wells where it lie in low impedance area. Also there are high amplitude in areas (A), (D) and (E).

2.4.2 Colored Inversion Results

In this part I will show the results of Colored inversion by running surface attributes for the reservoir interval which could give us a variety in viewing the results. This Figure (19,20 and 21) shows the presences of high P-impedance areas in the central part (B) and (C) which have hydrocarbon saturation and contain producer wells like WR-1, WR-5 and have a good structural trap but not all producer wells inside this trap. This impedance looks like two branches oriented NNE-SSW and NNW-SSE. In addition, there are two areas (A) and (D) to the west and to the east of producer wells, respectively, which give a high impedance that, could contain hydrocarbon but stratigraphically trapped.

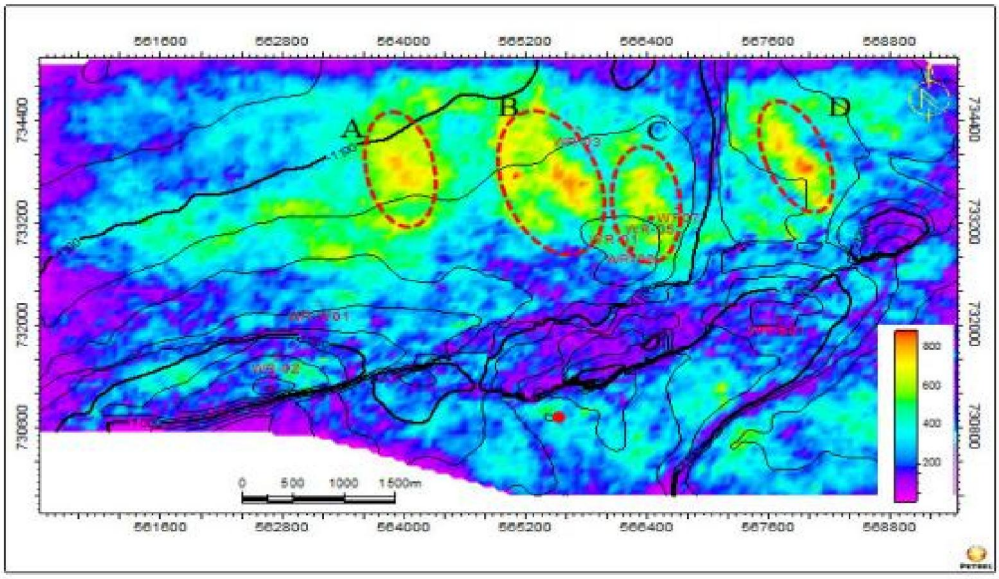

Figure (19): Relative P-Impedance slice (Arc length) on ARG-5, overlaid by TWT contours. This Figure shows the presences of high P-impedance areas in the central part (B) and (C) which have hydrocarbon saturation and contain producer wells like WR-1, WR-5 and have a good structural trap but not all producer wells inside this trap. This impedance looks like two branches oriented NNE-SSW and NNW-SSE. In addition, there are two areas (A) and (D) to the west and to the east of producer wells respectively, which give high impedance that, could contain hydrocarbon but stratigraphically trapped.

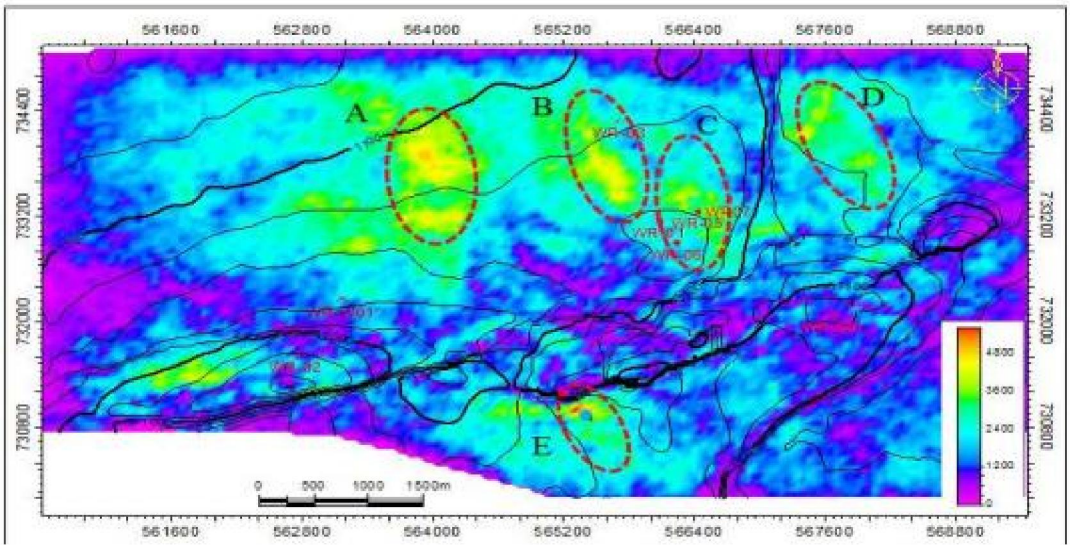

Figure (20): Relative P-Impedance slice (Average Magnitude) on ARG--5, overlaid by TWT contours. See the occurrence of high amplitude parts (B) and (C) which contain producer wells and (A), (D) and (E) areas which could contain hydrocarbon.

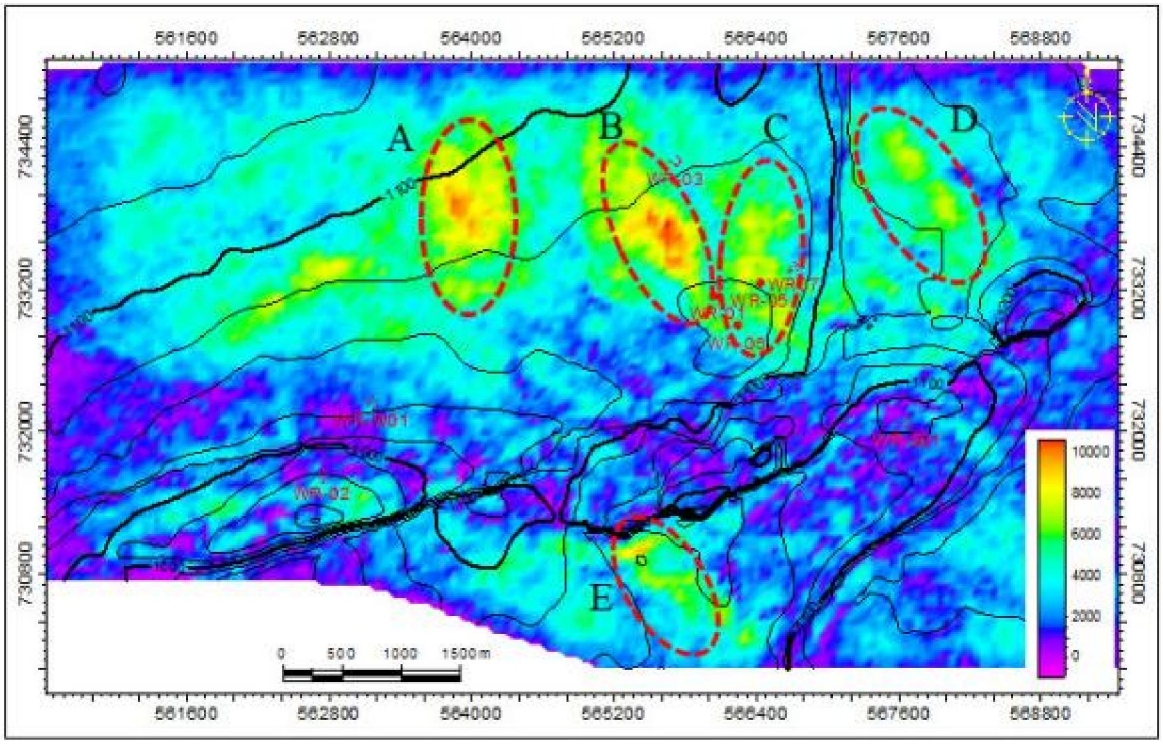

Figure (21): Relative P-Impedance slice (Maximum amplitude) on ARG-5, overlaid by TWT contours. There are high amplitude parts (B) and (C) where producer wells lie and (A), (D) and (E) areas which could contain hydrocarbon.

2.5 Neural Network Analysis

In its most general form, a neural network is a machine that is designed to model the way in which the brain performs a particular task or function of interest; the network is usually implemented by using electronic components or is simulated in software on a digital computer. Their main advantage over more traditional estimation methods is their ability to determine a nonlinear relationship between seismic properties and well log properties. This can be done by generating seismic attributes that are physically related to the reservoir properties and combining these attributes to predict the petrophysical properties of the reservoir (Hampson *et al.,* 2001).

2.5.1 Well Log Data Conditioning

In order for the well logs to be directly compared to the seismic data, a considerable amount of pre-processing was necessary. The main part of data conditioning workflow was described in chapter 3 but this is an additional conditioning, which is needed to prepare the data for the neural network. In this step, all well logs were converted from depth to time and the results are both resampled and smoothed to be consistent with the seismic data. The domain conversion step is easily performed by using a time-depth curve and spline interpolators, this is a critical step and the accuracy is needed. The resampling of the well-log data is needed because well-log sample intervals are much smaller than seismic sample intervals, many log samples will fall between two consecutive seismic samples after depth-to-time conversion. For this reason, a simple interpolation of the well log information on the sample times of the seismic data can produce well-log estimates affected by aliasing. This problem is addressed by resample the well-log data at seismic scale and low-pass filter the log data to limit their spectral content to that of the seismic data so that aliasing is avoided when down-sampling log data to the seismic resolution. Then we can apply the smoothing with low value to avoid any residual spikes. After many tries, the final parameters were; resample P-wave and Porosity logs to (4 ms.) as the seismic sample rate, and resample Water saturation log to (0.5 ms.), apply a low-pass filter to the Water saturation and porosity logs (90 Hz) and a high cut filter (100 Hz) and apply a low-pass filter to P-wave log (60 Hz) and a high cut filter (70 Hz), and smooth logs with a smoother length. In Figure (22) showing the validation error plot for Sw log for all wells. The minimum validation error occurs when a 1 point operator is used with 7 attributes (Black curve). Any other combination results in a larger validation error. This plot is important to determine the best number of attributes

and the operator length for each log. Figure (22) shows the outcome of the step-wise regression attained using a 1-point convolution operator. After the training of the data (Figure 23) cross-validation is used. In this process, each well is systematically removed from the training set and the transform is re-derived from the remaining wells (Figure 24). The prediction error for the hidden well is then calculated. The validation error, which is the average error for all hidden wells, is used as a measure of the likely prediction error when the transform is applied to the seismic volume. The prediction error is the RMS difference between the actual target log and the predicted target log.

	Target	Final Attribute	Training Error	Validation Error
1	Water Saturation	Y-Coordinate	0.193840	0.203828
2	Water Saturation	Derivative	0.187483	0.202296
3	Water Saturation	Colored inversion	0.177482	0.189594
4	Water Saturation	Filter 35/40-45/50	0.173655	0.189729
5	Water Saturation	Amplitude Weighted Frequency	0.170982	0.191694
6	Water Saturation	Integrate	0.166184	0.190562
7	Water Saturation	Dominant Frequency	0.161441	0.179242
8	Water Saturation	Quadrature Trace	0.159458	0.185626
9	Water Saturation	Filter 25/30-35/40	0.155191	0.192957
10	Water Saturation	Time	0.152968	0.184593
11	Water Saturation	Derivative Instantaneous Amplitude	0.150503	0.185834
12	Water Saturation	Filter 45/50-55/60	0.148507	0.205141
13	Water Saturation	Cosine Instantaneous Phase	0.147787	0.209000
14	Water Saturation	Instantaneous Phase	0.147460	0.210642
15	Water Saturation	Amplitude Weighted Phase	0.146993	0.212315

Figure (**22**): Step-wise regression results. The minimum Validation Error occurs with the Seventh attribute (Dominant frequency).

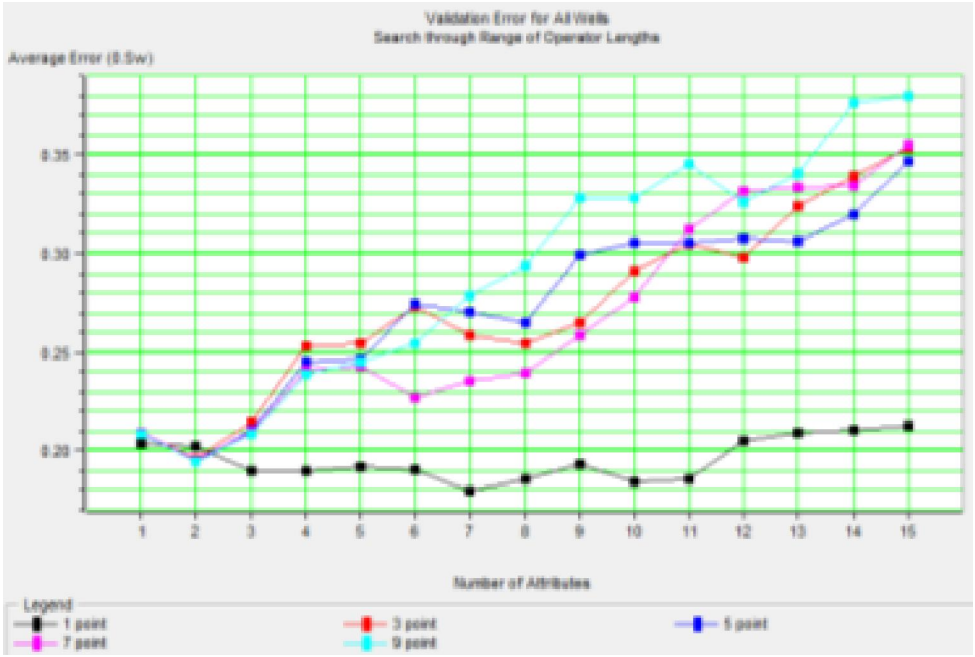

Figure (23): Validation error plot for different operator lengths. The minimum Validation Error occurs when a one point operator (black curve) is used with 7 attributes.

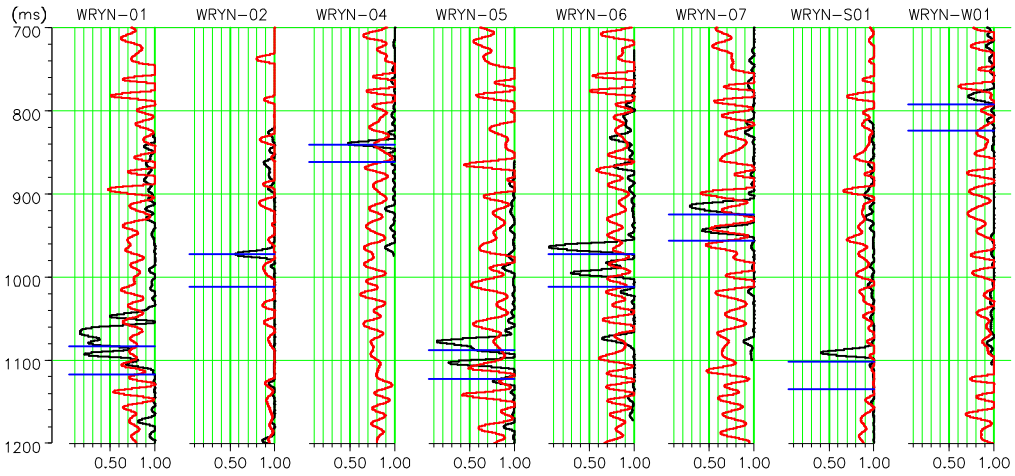

Figure (24): Validation of the multi-attribute linear regression at the training wells, in which the values at each well are predicted using the values from the other wells. The normalized correlation coefficient for all the wells is 0.52.

2.5.2 Neural Network Application

Neural network used to predict reservoir properties when the relationships between data are complex and non-linear. The following is the application of the PNN to derive S_w and PHIE. The basic idea behind the general regression probabilistic neural network is to use a set of one or more measured values, called independent variables, to predict the value of a single dependent variable.

2.6 Neural Network Results

The results from the multi-attribute linear regression approach and the neural networks suggest applying the PNN to the whole seismic volume using the attributes determined by the well trained. The results from neural network tries to suggest applying PNN network 6 to the whole seismic volume using the attributes determined by the well trained. The line shown here is a reconstructed cross-section through the volume intersecting 4 wells. Figures (25 and 26) show results data slices corresponding to porosity and water saturation respectively. Figure (25) shows a porosity distribution which gives good locations for high porosity which not coincides with the structure traps. In Figure (26), the hydrocarbon saturation didn't coincide with contour lines of the structural traps; i.e. there is a hydrocarbon but not only structurally controlled.

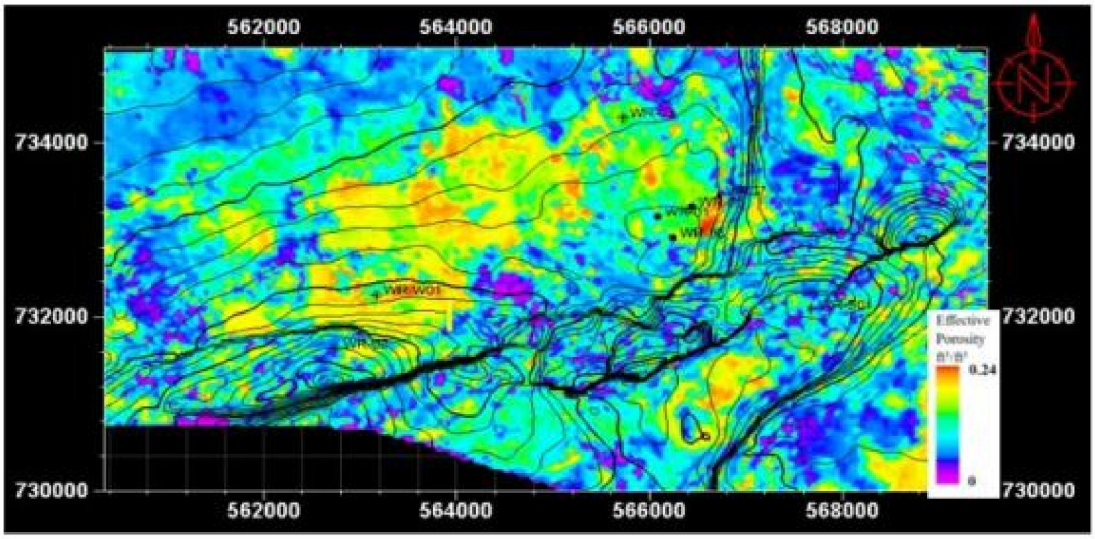

Figure (25): Porosity slice overlaid by the TWT contours for ARG-. The map shows porosity distribution all over study area.

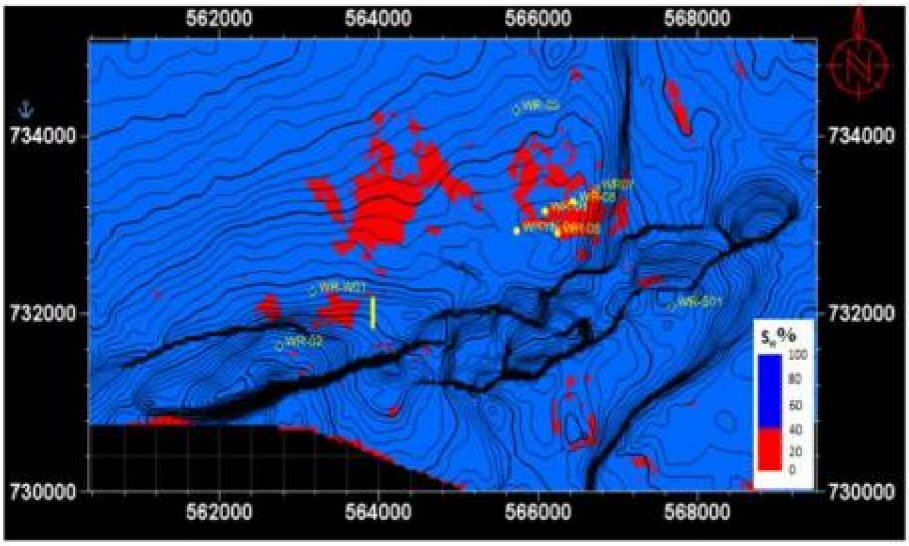

Figure (26): Water saturation slice overlaid by the TWT contours for ARG-5. The hydrocarbon saturation is 40% (in red) while the water saturation is 60% (in blue).

Conclusion

The results of post-stack inversion was only acoustic impedance (P-Impedance) so, there is no additional output for that inversion seismic attributes for the inverted P-impedance had been running there is a footprint for the presence of the hydrocarbon but also give new possible locations for drilling new producing wells based on finding the stratigraphic plays. In Neural Network, the prediction of S_w will have the ultimate effect of production enhancement and economic profitability.

Acknowledgements

We would like to thank the Egyptian General Petroleum Corporation (EGPC) for providing the data and for permission to publish this study. I also thank Prof. Dr. Adel A. A. Othman, Professor of Geophysics, for their constructive suggestions.

References

1. Abdel Aziz, M., Moustafa A. R. and Said, S. E., 1998, Impact of Basin inversion on hydrocarbon habitat in the Qarun concession, western desert, Egypt: 14th petroleum conference, 1, P. 139-155.
2. Dolson, J. C., M. V. Shann, U.K., Dr. H. Hammouda, R. Rashed, And Dr. S. Matbouly, 2000, the petroleum potential of Egypt, presented to the second wallace e. pratt memorial conference on petroleum provinces of the 21st century, San diego, California, January 12-15, 2000.
3. EGPC (1992): "Western Desert Oil and Gas Filed", 11th Exploration Conferences, Cairo, Egypt, p.431.
4. Hampson, D. P., Schuelke, J.S., Quirein, J.A., 2001, "Use of multiattribute transforms to predict log properties from seismic data", Geophysics, January-February, Vol. 66, No. 1, p. 220-236.
5. Hantar, G., 1990, North Western Desert, Egypt. In: The Geology of Egypt (Ed. R. Said), Chapter 15, P. 293 – 320.
6. Kemper, M., 2010, Rock physics driven inversion: the importance of workflow, First Break, 28, p. 69-81.
7. Krenkel, H., 1925, Geologie Afrikas: Verlag von. Gebruder, Berlin, p. 461.
8. Moustafa, A. R., 2008, Mesozoic-Cenozoic Basin Evolution in the Northern Western Desert of Egypt: Geology of East Libya, vol. 3, pp. 29-46.
9. Moustafa, A. R., and Khalil, M. H., 1988: Structural characteristics and tectonic evolution of north Sinai fold belts, in: The Geology of Egypt (Ed. R. Said),
10. Pendrel, J. and Geosystems, J., 2001, Seismic Inversion – The Best Tool for Reservoir Characterization, CSEG Recorder.
11. Russell, B. and Hampson, D., 2006, the old and the new in seismic inversion, CSEG Recorder, December, p. 5-11.
12. Said, R., 1990, Cenozoic, Egypt. In: The Geology of Egypt (Ed. R. Said), Chapter 24, P. 451 – 486.
13. Veeken, P. C. H., and Silva, M. D., 2004, Seismic inversion methods and some of their constraints, First Break 22, p. 47-70.

1/12/2016